Effect of isotope disorder on the Raman spectra of cubic boron arsenide

Akash Rai[1], Sheng Li,[2] Hanlin Wu,[2] Bing Lv[2], and David G. Cahill[1]

[1]*Department of Materials Science and Engineering and Materials Research Laboratory, University of Illinois at Urbana-Champaign, Urbana, Illinois 61801, USA*

[2]*Department of Physics, University of Texas at Dallas, Richardson, Texas 75080, USA*

Boron arsenide (*c*-BAs) is at the forefront of research on ultrahigh thermal conductivity materials. We present a Raman scattering study of isotopically tailored cubic boron arsenide single crystals for 11 isotopic compositions spanning the range from nearly pure *c*-^{10}BAs to nearly pure *c*-^{11}BAs. Our results provide insights on the effects of strong mass disorder on optical phonons and the appearance of two-mode behavior in the Raman spectra of mixed crystals. Strong isotope disorder also relaxes the one-phonon Raman selection rules, resulting in disorder-activated Raman scattering by acoustic phonons.

I. INTRODUCTION

In 2013, first-principles calculations by Lindsay *et al.* predicted a remarkable room temperature thermal conductivity (κ) for cubic boron arsenide (*c*-BAs) of 2200 W/m K, comparable to that of diamond [1]. This calculation [1] considered only lowest order anharmonicity. The high room temperature κ was attributed to significantly suppressed three-phonon scattering in *c*-BAs due to a combination of a large frequency gap between acoustic and optical modes (a-o gap), bunching of acoustic branches, and relatively small optical phonon bandwidth [1]. More recent computational studies that include the next higher order term in the anharmonicity found that significant four-phonon scattering in *c*-BAs reduces the predicted thermal conductivity at room temperature to 1400 W/m K [2,3]. The experimental value is approximately 1000 W/m K [4–6].

In this work, we examine another extreme property of the lattice dynamics of *c*-BAs: The effect of strong isotope disorder on the vibrational modes cannot be described by the weak-scattering limit of the coherent potential approximation (CPA) that is typically successful in predicting the frequencies and lifetimes of optical phonons in isotopically modified crystals [7,8]. The strong deviation from virtual crystal behavior in *c*-BAs was identified in a 2013 study of the vibrational Raman spectra for natural isotope abundance and ^{11}B isotopically enriched crystals [9]. Hadjiev *et al.* investigated this anomalous two-mode behavior by analyzing density functional perturbation theory (DFPT) simulations that reproduce the experimental properties of *c*-BAs [9]. However, the theoretical methods used previously [8,9] for studying the isotopic mass disorder, within the framework of the CPA, fail to explain the localized vibrational modes seen in *c*-BAs. Experimental studies of systematically varied isotopically disordered crystals is necessary to build a deeper understanding of the anomalous vibrational behavior not seen in previously known isotopically disordered binary compounds. Here, we

present an experimental Raman study of 11 *c*-BAs isotopically mixed crystals with isotope compositions that span the range from nearly pure *c*-^{10}BAs to nearly pure *c*-^{11}BAs. The large number of compositions allows us to examine how the Raman spectra evolve as a function of mass disorder.

Within the harmonic approximation, the Raman frequency shift (ν) of the zone-center optical phonon of a homogeneous crystal scales inversely as the square root of the reduced mass (μ) of the two atoms that make up the basis of atoms in a zinc-blende or wurtzite crystal structure:

$$\nu \propto \mu^{-1/2}. \tag{1}$$

Within the weak-scattering limit of the coherent potential approximation (CPA), this scaling law can be modified to account for isotope disorder and anharmonicity through a phonon self-energy term. This phonon self-energy has real, and imaginary, parts related to the phonon frequency shift, and spectral broadening, respectively [8]. Phonon self-energies due to isotopic disorder have been extensively studied [7–11]. Phonons in a homogeneous crystal have infinite lifetime in the harmonic approximation. In a real crystal with no isotopic disorder, the phonon lifetime is finite due to anharmonicity and the phonon line shape is Lorentzian. The Lorentzian line shape is slightly distorted in the presence of isotope disorder.

A comprehensive Raman study by Cardona and co-workers described the effect of isotopic disorder on the lattice dynamics of several elemental and compound semiconductors (Widulle *et al.* [8]). They calculated the self-energies due to isotopic disorder and obtained a detailed picture of the phonon renormalization by simulating line shape properties within the framework of the CPA. More recent theoretical calculations by Mahan derived the effect of atomic isotopes on the phonon modes of a crystal and concluded that in solving for the vibrational modes, mixing of modes by isotope scattering is an important process [12].

The vibrational properties of cubic boron arsenide with natural isotope abundance (^{nat}BAs) and cubic boron arsenide

isotopically enriched with ^{11}B (^{11}BAs) were studied by Hadjiev *et al.* using Raman spectroscopy and first-principles density functional perturbation theory (DFPT) [9]. In ^{nat}BAs, they observed an anomalous two-mode behavior not seen in other isotopically disordered crystals; they tentatively attributed this behavior to the localization of ^{10}B vibrational states. They also observed a lack of LO-TO splitting in the measured Raman spectrum of ^{11}BAs and further investigated the small LO-TO splitting in ^{nat}BAs using DFPT [9]. The calculated phonon dispersion of c-BAs includes overbending of the upmost optical phonon branch [9]; i.e., the frequency of phonons on the nondegenerate optical branch is higher than that of the zone-center phonon, similar to the optical phonon dispersion of diamond [13]. They evaluated the real part of phonon self-energy in ^{nat}BAs arising due to isotopic disorder at the zone center as $\Delta_{dis} \approx -3\,\mathrm{cm}^{-1}$, with small disorder-induced broadening $\Gamma_{dis} \approx 0.4\,\mathrm{cm}^{-1}$ [9].

The two-mode behavior seen in the Raman spectra of ^{nat}BAs is often observed in mixed crystals of the type $LM_{1-x}N_x$, where the Raman frequencies of the LM and LN (Fig. 1) components differ significantly [14–16]. At intermediate compositions x, two sets of frequencies are often observed; one set of frequencies is related to the LO and TO modes of the lighter LM component, and the other set of frequencies is related to the LO and TO modes of the heavier LN component [16,17]. There have been numerous attempts to provide a theoretical criterion for predicting one- or two-mode behavior in mixed diatomic crystal. These criteria are extensively reviewed by Sen and Hartmann [18].

Chang and Mitra proposed a modified random-element isodisplacement (MREI) model that assumed that all cation-anion pairs vibrate in phase, as in the $k = 0$ optic mode of a perfect diatomic crystal [14]. This leads to a criterion for two-mode behavior depending only on the masses of constituents,

$$m_M^{-1} > m_L^{-1} + m_N^{-1}. \qquad (2)$$

Here, $\mu_{LN}^{-1} = m_L^{-1} + m_N^{-1}$ is the reduced mass of the compound LN.

This criterion states that a mixed crystal that displays two-mode behavior has a substituting atom with a mass smaller than the reduced mass of the compound formed by the other two atoms. They successfully applied this criterion to predict one- and two-mode behavior in various mixed crystals [14]. Figure 1 shows the summary of this condition tested on mixed crystals by Chang and Mitra together with c-^{10}B$_{1-x}$^{11}B$_x$As, i.e., a ^{10}B impurity in ^{11}BAs. The dashed line represents the condition stated in Eq. (2) and forms a separating boundary between one- and two-mode behaviors in mixed crystals. As seen in Fig. 1, c-BAs lies almost exactly on the dashed line and is therefore at the cusp of satisfying this condition of two-mode behavior.

II. EXPERIMENT

We synthesized single crystals of isotopically tailored c-BAs by a modified chemical vapor transport (CVT) method using I$_2$ as the transport agent [5]. The B source materials, ^{10}B powder (Alfa Aesar, 99.9% chemical purity and > 96 at. % ^{10}B), and ^{11}B powder (Alfa Aesar, 99.9% chemical purity
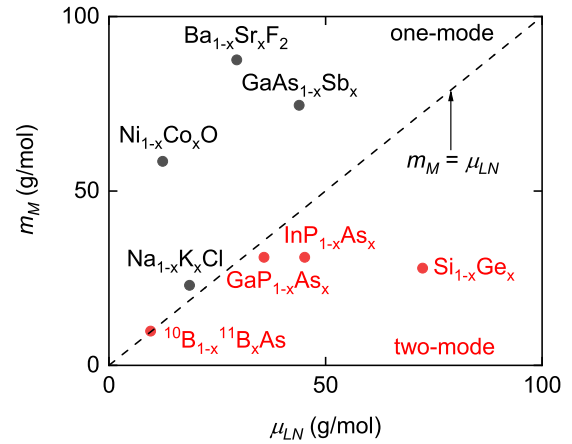

FIG. 1. Summary of the two-mode behavior criterion [Eq. (2)] proposed by Chang and Mitra [14], tested on selected mixed crystals of the type $LM_{1-x}N_x$ (mixture of the compound LM and the compound LN) along with c-^{10}B$_{1-x}$^{11}B$_x$As (^{10}B substituting in ^{11}BAs). The y axis is the mass of the substituting element M (m_M) and the x axis is the reduced mass (μ_{LN}) of the compound LN. One-mode behavior mixed crystals: LN-arbitrary binary compound with element L (O, Cl, Ga, F$_2$) and N (K, Co, Sr, Sb). LM-arbitrary binary compound with element L (O, Cl, Ga, F$_2$) and M (N, Ni, Ba, As). For mixed crystals of type $LM_{1-x}N_x$, LM is the lighter and LN is heavier compound. The dashed line represents the condition $m_M = \mu_{LN}$ and forms a separating boundary between one- and two-mode crystals. The behavior of mixed crystals is drawn from Ref. [14].

and >96 atomic% ^{11}B), were mixed with the molar ratio of ^{10}B:^{11}B $= x : 1–x$ (x varies from 0 to 1 at intervals of 0.1). The B powder was mixed with As chunks (Alfa Aesar, 99.999%) with the atomic ratio of B : As $= 1 : 7$. The mixture of B and As source materials was then sealed in an evacuated quartz tube together with a small amount (typically $1.2\,\mathrm{mg\,cm}^{-3}$ of the volume of the container) of the transport agent (I$_2$). The end of the quartz tube containing the source materials was placed at the high temperature zone of a horizontal furnace at $900\,°$C. The cold zone of the quartz tube was placed at the lower temperature zone of the furnace at $800\,°$C. Crystal growth proceeded over the course of 3 weeks. The synthesized single crystals of c-BAs had a lateral dimension on the order of 0.5 mm and growth facets parallel to the {111} planes.

The isotopic composition of the c-BAs crystals deviates from the nominal composition likely due to the differences of transfer rate during the CVT process caused by the sizes and morphologies of the ^{10}B and ^{11}B powders and is determined using time-of-flight secondary ion mass spectroscopy (TOF SIMS). Before measurement, we clean the c-BAs single crystals by ultrasonication in ethanol followed by distilled water for 3 min each. We then ion polish a {111} growth facet for 5 min using a GATAN PECS II ion polishing system. The operating parameters of the ion polishing system are an Ar ion energy of 6 keV, ion gun current of 45 μA, and grazing incidence angle of $3\,°$.

Raman spectroscopy measurements are performed using a custom-built optical system based on an Acton Insight spectrometer (Princeton Instruments). The excitation wavelength is 488 nm from a Spectra-Physics cyan laser. The excitation laser is focused by a $20\times$, NA $= 0.4$, objective lens. The
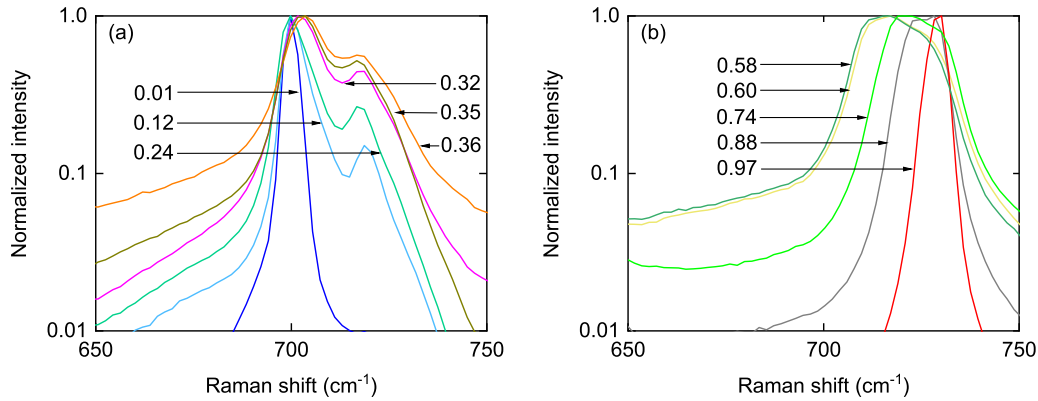
FIG. 2. Raman spectra of isotopic mixed crystals of $^{10}B_x{}^{11}B_{1-x}As$ for (a) $0 < x < 0.4$, and (b) $0.5 < x < 1.0$. The spectra are measured at room temperature with 488-nm laser excitation on {111} growth facets in a backscattering geometry. The measured Raman intensity is normalized by the maximum intensity of the spectrum for each sample. The y axis is logarithmic.

laser power on the sample is ≈ 6 mW and the $1/e^2$ intensity radius of the focused laser beam is ≈ 5 μm. The backscattered Raman light is collected through the same objective and dispersed by a 1200 mm^{-1} grating. The spectrometer is calibrated using a Si wafer. The frequency shift of the Raman active optical phonon in Si at room temperature is 520 cm^{-1} [19]. We assume a linear relationship between pixel number and Raman shift. We verified our calibration by measuring Raman scattering by O_2 molecules in the air adjacent to an Al-coated sample. We measure the O_2 stretching vibrational mode frequency as 1555 cm^{-1}, within 0.1% of the expected value of 1556.2 cm^{-1} [20].

The expected measured line shape of a Raman peak is the convolution of a Lorentzian phonon line shape with the Gaussian response function of the spectrometer. The convolution of a Lorentzian with a Gaussian is a Voigt profile [21]. An approximation for the relation between the full width at half maximum (FWHM) widths of the Voigt (f_v), Gaussian (f_G), and Lorentzian (f_L) profiles is given by [22]

$$f_v \approx 0.535 f_L + \sqrt{0.217 f_L^2 + f_G^2}. \tag{3}$$

The FWHM of a Voigt profile fit to experimental data for the Raman peak of Si in our Raman spectrometer is 5.4 cm^{-1}. The Voigt profile can be deconvoluted to find the width of the Gaussian spectrometer response function using the previously determined Lorentzian line shape of Si. The intrinsic FWHM of the Si Raman line is 2.6 cm^{-1} at room temperature [23,24]. The Gaussian FWHM due to instrumental broadening alone is 3.9 cm^{-1}.

III. RESULTS AND DISCUSSION

Figure 2 shows the normalized Raman spectra of isotopically tailored cubic boron arsenide single crystals from 650 to 750 cm^{-1} with ^{11}B-rich [panel (a)] and ^{10}B-rich [panel (b)] compositions. The Raman spectrum for nearly pure ^{11}BAs has a single symmetric peak corresponding to the Raman active longitudinal optical (LO) vibrational mode at the zone center. We label the peak that we associate with ^{11}B-related vibrational modes as P1. The Voigt profile fit to P1 for nearly pure ^{11}BAs ($x = 0.01$) is shown in Fig. 3(a). After deconvolution

by the instrument resolution function, the Lorentzian FWHM of this peak is 1.2 ± 0.2 cm^{-1} corresponding to an optical phonon lifetime of 4.4 ± 0.6 ps [25].

As isotope disorder increases in ^{11}B-rich crystals [see Fig. 2(a)], the P1 peak broadens, and a second peak, labeled P2, appears where the phonon densities of states of ^{11}BAs and ^{10}BAs overlap [9]. In the previous study of natural isotope abundance c-BAs by Hadjiev et $al.$, the P2 peak was attributed to localized ^{10}B-related optical modes [9]. A recent study on localization of phonons in mass-disordered alloys have shown that for binary isotopic disorder, light impurities can induce localized modes beyond the bandwidth of the host system [26]. The observed two-mode behavior is also consistent with the Chang and Mitra criterion discussed above [Eq. (2)] [14].

The Raman spectrum for nearly pure ^{10}BAs crystals has a single symmetric P2 peak, corresponding to the Raman active LO optical phonons at the zone center. The Voigt profile fit to P2, after deconvolution by the instrumental resolutions, yields a Lorentzian FWHM of 1.5 ± 0.3 cm^{-1}. This linewidth corresponds to an optical phonon lifetime of 3.6 ± 0.5 ps [25]. As x decreases from 0.97 to 0.58, i.e., as ^{11}B is substituted for ^{10}B, the P2 peak broadens and a P1 peak appears. We conclude that the two-mode behavior observed in ^{nat}BAs by Hadjiev et $al.$ [9] is observed for all isotopic compositions of c-$^{10}B_x{}^{11}B_{1-x}As$ except the compositions that are nearly isotopically pure, $x = 0.01$ and $x = 0.97$.

Figure 4 summarizes the positions and widths of peaks P1 and P2 as a function of isotopic composition. Since the LO-TO splitting is smaller than our instrument resolution, at any intermediate compositions x, only two frequencies are observed; one frequency is related to the optical vibrational modes of the lighter ^{10}B-like vibrations (peak P2), and the other frequency is related to the optical vibrational modes of the heavier ^{11}B-like vibrations (peak P1). The dashed line in Fig. 4(a) shows the expected mean-field dependence of the optical phonon frequency on the composition through the reduced mass [Eq. (1)]. For a binary compound, the mean field scaling of Raman frequency only strictly holds for the zone-center vibrational mode [8]. Nevertheless, the position of peak P1 compares well with the expected mean field scaling with the square root of reduced mass. The position of peak
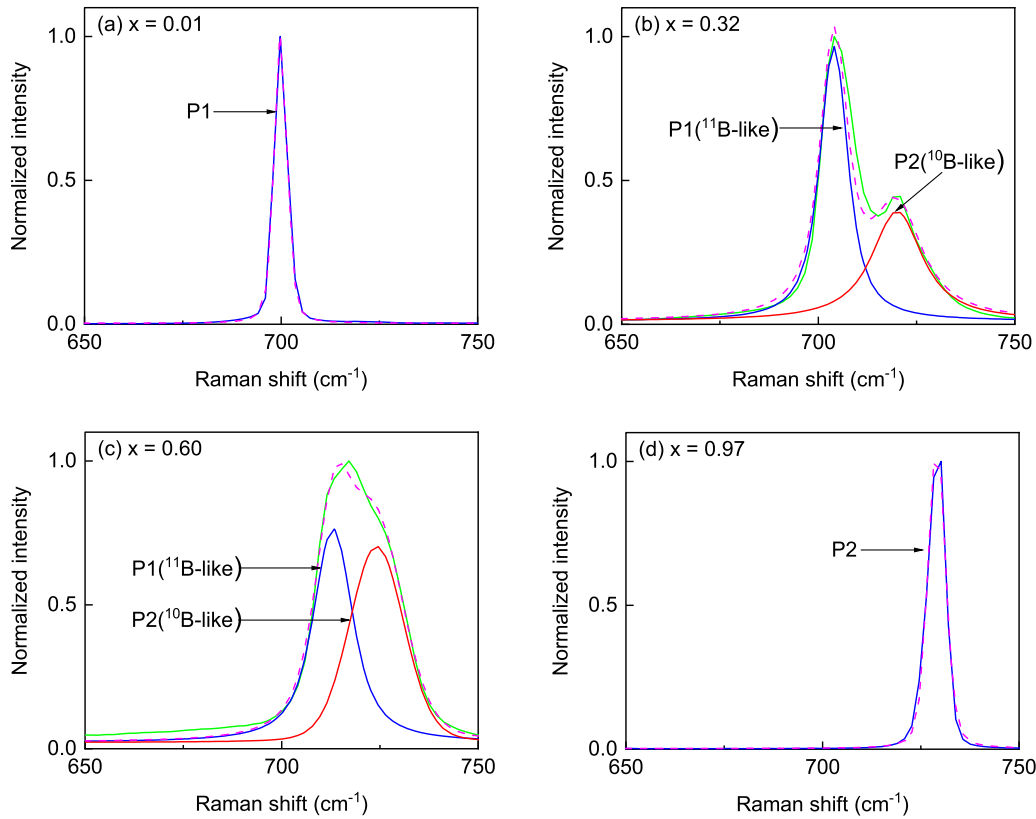
FIG. 3. The Raman spectra of compositions (a) $x = 0.01$, (b) $x = 0.32$, (c) $x = 0.60$, and (d) $x = 0.97$ are replotted. The experimental data shown as solid lines and fits to a symmetric Voigt profile are shown as dashed lines. The measured spectra are fit to multiple peaks. We attribute peaks P1 (blue) and P2 (red) to ^{11}B-related and ^{10}B-related vibrational modes, respectively.

P2, however, does not follow the same trend. The trend in the Raman shift of the peaks P1 and P2 as a function of isotopic composition is reminiscent of the two-mode behavior observed in mixed crystals that satisfy the Chang and Mitra criteria [14].

Within the framework of the weak-scattering limit of the coherent potential approximation (CPA), the spectral broadening of the Raman peak of an isotopically disordered crystal is due to the decrease in the phonon lifetime caused by mass disorder; the broadening is expected to increase with the
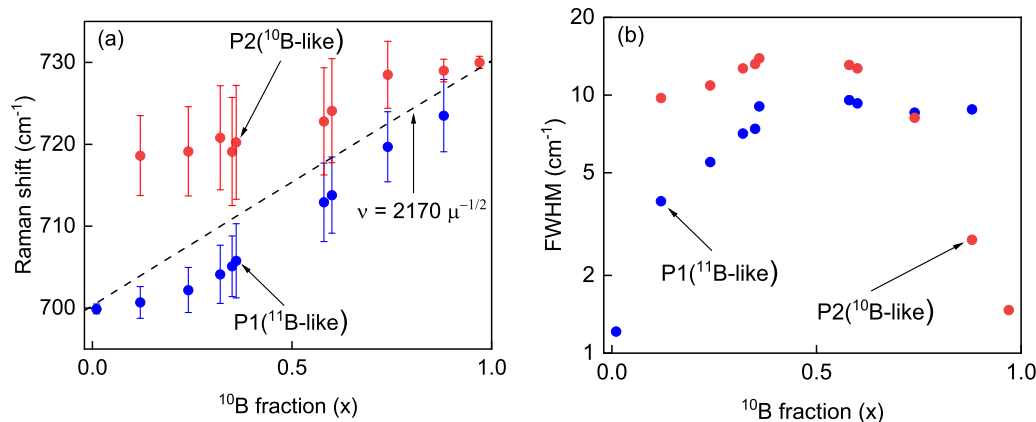

FIG. 4. (a) The measured Raman shift (ν) corresponding to peaks P1 (blue data points) and P2 (red data points), due to ^{11}B-like and ^{10}B-like optical vibrational modes, respectively, with respect to ^{10}B isotopic composition (x). The dashed line indicates the expected scaling of the zone-center optical phonon frequency with the reduced mass (μ); see Eq. (1). For each isotopic composition, the Lorentzian and Gaussian FWHM of P1 and P2 can be estimated by fitting the experimental data with Voigt profile fit and deconvoluting by the Gaussian instrumental broadening. In panel (a), the Lorentzian FWHM of P1 and P2 are depicted as error bars surrounding the peak Raman shift for each composition. In panel (b), the Lorentzian FWHM of P1 (blue data points) and P2 (red data points) are plotted as a function of ^{10}B composition (x). The y axis of panel (b) is logarithmic.

increasing isotopic mass disorder and reach a maximum at $x = 0.5$. Hadjiev *et al.* calculated the disorder-induced broadening within the CPA and found an extremely small broadening of $0.4 \, \text{cm}^{-1}$ [9]. The Lorentzian FWHM of both peaks P1 and P2 is estimated by fitting the data to a symmetric Voigt profile and deconvoluting the Voigt profile with the instrumental resolution function. The Lorentzian FWHM of P1 and P2 derived from this procedure is summarized in Fig. 4(b).

For isotopically disordered *c*-BAs crystals, the observed broadening is nearly two orders of magnitude larger and therefore cannot easily be attributed to changes in optical phonon lifetime that are produced by mass disorder. Also, the broadening cannot be attributed to anharmonicity. The three-phonon Klemens mechanism [27] is not active in *c*-BAs due to the large gap between the frequency of the highest frequency acoustic phonons and the low frequency optical phonons [9]. Based on first-principles calculations by Feng *et al.*, inclusion of four-phonon scattering reduces the room temperature optical phonon lifetime from 10^4 to $40 \, \text{ps}$ [2]. Thus, major contribution to phonon renormalization effects comes from fourth order anharmonicity, through a decay of a T_2 optical phonon into three acoustic phonons (O→3A) [8,9]. Hajidev *et al.* employed a model for this decay channel where a T_2 optical phonon with frequency (ν_0) decays into three acoustic phonons each with frequency ($\nu_0/3$) and a calculated small contribution to spectral broadening of $0.4 \, \text{cm}^{-1}$ [9]. Thus, the observed large spectral broadening with increasing isotopic disorder cannot be attributed to the contributions from isotopic mass disorder and anharmonicity alone. Disorder-activated one-phonon optical Raman scattering due to mass disorder and concomitant *k*-vector relaxation may contribute significantly to the spectral broadening.

We also observe disorder-activated Raman scattering where the usual crystal momentum selection rules are partially relaxed and phonon frequencies with a high density of states appear in the one-phonon Raman spectra. We plot the low frequency region of the Raman spectra in Fig. 5(a). In an isotopically disordered sample with compositions $x = 0.24$, 0.36, 0.60, and 0.74, we observe peaks corresponding to TA (*L*) at $132 \, \text{cm}^{-1}$, TA (*W*) at $218 \, \text{cm}^{-1}$, and LA (*W*) at $275 \, \text{cm}^{-1}$. The frequencies of the acoustic phonons do not shift significantly with B isotopic composition and therefore we expect these disorder-activated to be independent of isotopic composition. The high densities of states at these frequencies are apparent in the phonon density of states calculated by density functional perturbation theory and plotted in Fig. 5(b). We also observe a weak peak in the data for all compositions at $394 \, \text{cm}^{-1}$, corresponding to two-phonon Raman scattering from transverse acoustic phonons with crystal momentum near the *X* point.

A similar feature is observed in the one-phonon optical Raman spectra of ^{10}B-rich compositions plotted in Fig. 6(a). We observe peaks that we tentatively attribute to disorder-induced one phonon Raman scattering about 50–$90 \, \text{cm}^{-1}$ below the zone-center Raman peak. In an isotopically disordered sample with compositions $x = 0.58$, 0.60, 0.75, 0.88, and 0.97, we observe peaks corresponding to ^{10}B-like TO(*W*) + TO(*K*) vibrational modes at $\approx 646 \, \text{cm}^{-1}$. For the composition $x = 0.97$ this disorder-induced peak is relatively narrow and weak. With increasing isotopic disorder from $x = 0.97$ to $x = 0.58$, this
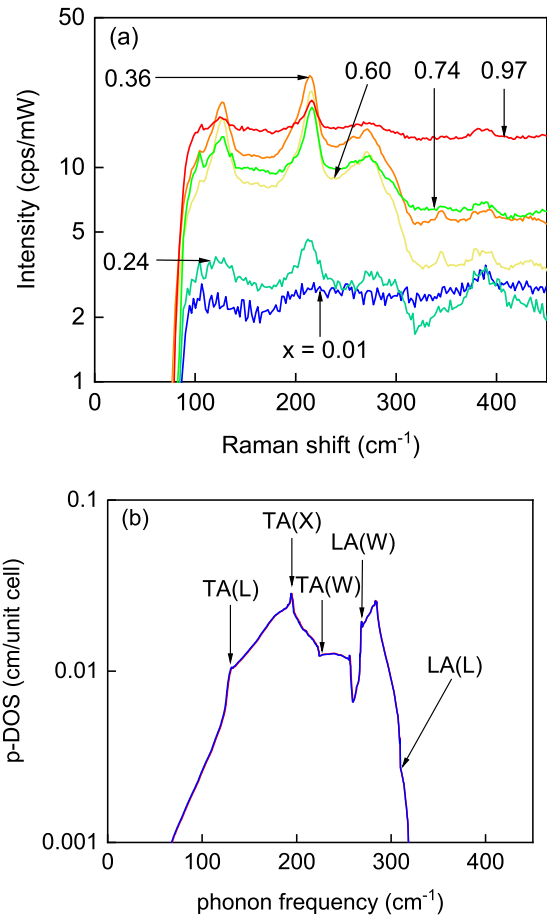

FIG. 5. (a) Measured Raman spectra of low frequency acoustic phonons in c-^{10}B$_x^{11}$B$_{1-x}$As for various ^{10}B compositions (x). The intensity in counts per second is normalized by the power of the 488-nm laser excitation in mW units. (b) Calculated phonon density of states (p-DOS) showing critical points associated with transverse acoustic (TA) and longitudinal acoustic (LA) phonons at points on the Brillouin zone boundaries, *W*, *X*, and *L*. Isotopically tailored crystals show disorder-induced Raman scattering from acoustic phonons which are not seen in the isotopically enriched crystal ($x = 0.01$ and 0.97). The most prominent features are scattering by the TA phonons at the *L* and *X* points. The *y* axes of both panels (a) and (b) are logarithmic.

peak broadens and becomes stronger in relative intensity as we expect. We do not observe a shift in the frequency of this peak with B isotopic composition and it is close to the expected peak in the optical phonon density of states corresponding to TO(*W*) + TO(*K*) at $646 \, \text{cm}^{-1}$ for $x = 1.0$. This is shown in Fig. 6(b), where the optical phonon density of states calculated by density functional perturbation theory is plotted against phonon frequency. The experimentally observed shift in wave vector at the Γ point of the ^{10}B-enriched crystal ($x = 0.97$) compared to the ^{11}B-enriched crystal ($x = 0.01$) is $\approx 30 \, \text{cm}^{-1}$, is very close to the calculated shift in the phonon density of states with the reduced mass of crystal $\approx 32 \, \text{cm}^{-1}$.

Finally, we discuss the effects of strong isotopic disorder on the high frequency regime of the Raman spectra that includes Raman scattering by combinations of two optical phonons; see Fig. 7(a). We compare our Raman scattering
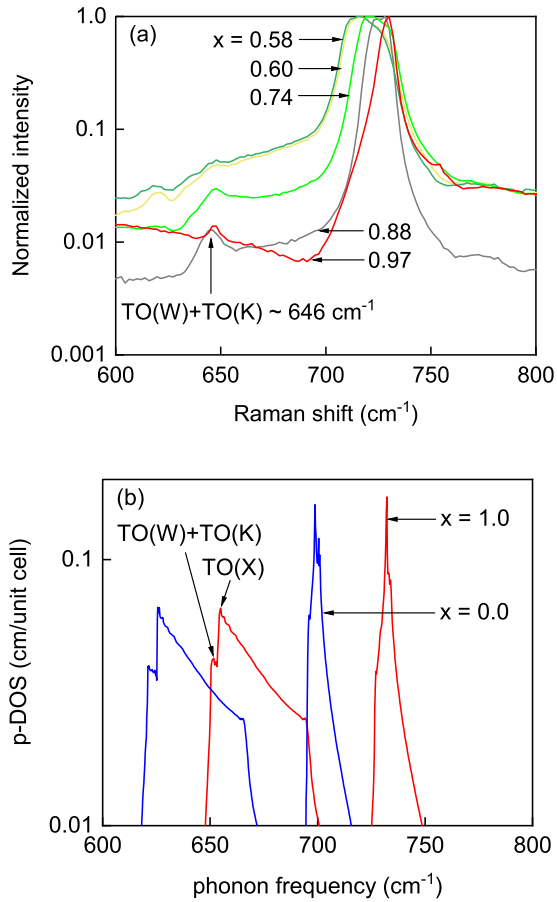
FIG. 6. (a) Measured Raman spectra of ^{10}B-rich compositions c-^{10}B$_x$^{11}B$_{1-x}$As in the frequency regime that involves Raman scattering from one optical phonon. The intensity in counts per second is normalized by the power of the 488-nm laser excitation in mW units. Disorder-induced excitations for various ^{10}B-rich isotopically disordered crystals can be seen on the low energy tail of the Raman peak corresponding to the ^{10}B-like TO(W) +TO(K) vibrational mode at 646 cm^{-1}. (b) Optical phonon density of states (p-DOS) calculated by density functional perturbation theory plotted against the phonon frequency to facilitate comparison with the experiment data in panel (a).
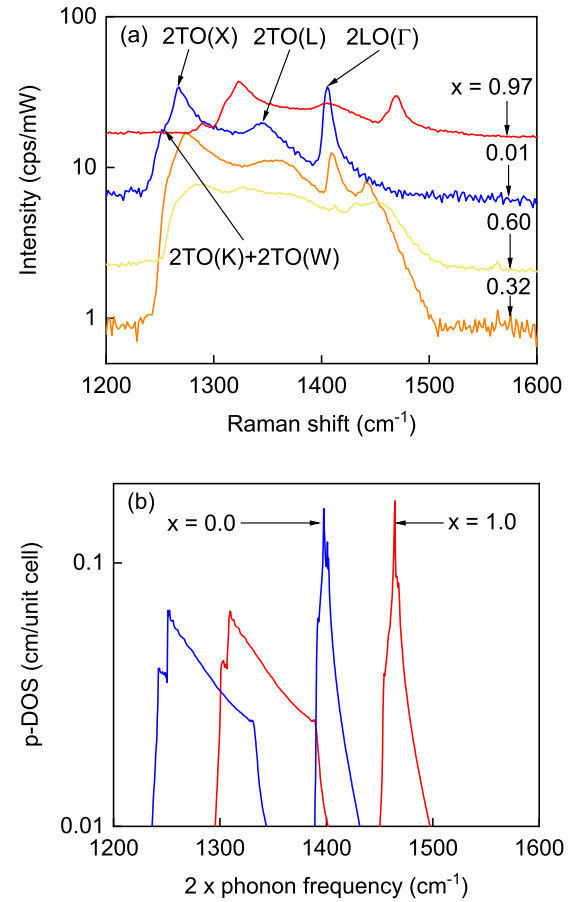
FIG. 7. (a) Measured Raman spectra in the high frequency regime that involves Raman scattering from combinations of two optical phonons. The intensity in counts per second is normalized by the power of the 488-nm laser excitation in mW units. (b) Optical phonon density of states (p-DOS) calculated by density functional perturbation theory plotted against twice the phonon frequency to facilitate comparison with the experiment data in panel (a).

data to calculations of the optical phonon density of states (p-DOS) in Fig. 7(b) where we have plotted the p-DOS against twice the phonon frequency. The second order spectra of the ^{11}B-enriched crystal ($x = 0.01$) shows two-phonon Raman scattering peaks corresponding to contributions from 2TO(K) and 2TO(W) at 1253 cm^{-1}, 2TO(X) at 1267 cm^{-1}, 2TO(L) at 1348 cm^{-1}, and 2LO(Γ) at 1405 cm^{-1}. These two-phonon peaks are less prominent in the ^{10}B-enriched crystal ($x = 0.97$) due to a larger background in the Raman intensities that we attribute to Raman scattering by free carriers. The experimentally observed shift in wave vector at the Γ point of ^{10}B-enriched crystal ($x = 0.97$) compared to ^{11}B-enriched crystal ($x = 0.01$) is ≈ 52 cm^{-1}, smaller but comparable to the calculated shift in the phonon density of states with the reduced mass of the crystal ≈ 65 cm^{-1}.

Raman scattering productively probes the high energy and high momentum carrying optical phonon modes near the Γ point. In ultrahigh thermal conductivity material such as c-

BAs, where anharmonicity is very weak due to dispersion features (e.g., phonon band gap, acoustic bunching [1]), the heat carrying high frequency acoustic phonons are not significantly scattered by the optical phonons at room temperature. While Raman based techniques can be used as a robust tool to study the thermal transport in materials where the acoustic phonon lifetime is significantly affected by optical phonons, the anomalous dispersion features of c-BAs prohibit a direct connection between the Raman results and thermal conductivity.

IV. CONCLUSION

In summary we have studied the effect of isotope disorder on the vibrational spectra of isotopically tailored c-BAs single crystals using Raman spectroscopy at room temperature. The two-mode behavior that is predicted by the Chang and Mitra criterion for the substitution of ^{10}BAs in ^{11}BAs is most clearly observed for ^{11}BAs-rich compositions. For ^{10}BAs-rich compositions, the two-mode behavior is not well developed because the spacing in frequency between the two modes is of the same order as their width.

[1] L. Lindsay, D. A. Broido, and T. L. Reinecke, Phys. Rev. Lett. **111**, 025901 (2013).

[2] T. Feng, L. Lindsay, and X. Ruan, Phys. Rev. B **96**, 161201(R) (2017).

[3] N. K. Ravichandran and D. A. Broido, Phys. Rev. X **10**, 021063 (2020).

[4] J. S. Kang, M. Li, H. Wu, H. Nguyen, and Y. Hu, Science **361**, 575 (2018).

[5] S. Li, Q. Zheng, Y. Lv, X. Liu, X. Wang, P. Y. Huang, D. G. Cahill, and B. Lv, Science **361**, 579 (2018).

[6] F. Tian, B. Song, X. Chen, N. K. Ravichandran, Y. Lv, K. Chen, S. Sullivan, J. Kim, Y. Zhou, T.-H. Liu *et al.*, Science **361**, 582 (2018).

[7] M. Cardona and T. Ruf, Solid State Commun. **117**, 201 (2001).

[8] F. Widulle, T. Ruf, M. Konuma, I. Silier, M. Cardona, W. Kriegseis, and V. Ozhogin, Solid State Commun. **118**, 1 (2001).

[9] V. G. Hadjiev, M. N. Iliev, B. Lv, Z. F. Ren, and C. W. Chu, Phys. Rev. B **89** 024308, (2014).

[10] S.-I. Tamura, Phys. Rev. B **27**, 858 (1983).

[11] S.-I. Tamura, Phys. Rev. B **30**, 849 (1984).

[12] G. D. Mahan, Phys. Rev. B **100**, 024307 (2019).

[13] P. Pavone, K. Karch, O. Schutt, W. Windl, D. Strauch, P. Giannozzi, and S. Baroni, Phys. Rev. B **48**, 3156 (1993).

[14] I. F. Chang and S. S. Mitra, Phys. Rev. **172**, 924 (1968).

[15] G. Lucovsky, M. H. Brodsky, and E. Burstein, Phys. Rev. B **2**, 3295 (1970).

[16] L. Bergman and R. J. Nemanich, Annu. Rev. Mater. Sci. **26**, 551 (1996).

[17] L. Genzel and W. Bauhofer, Z. Phys. B: Condens. Matter **25**, 1 (1976).

[18] P. Sen and W. Hartmann, Phys. Rev. B **9**, 367 (1974).

[19] K. Uchinokura, T. Sekine, and E. Matsuura, Solid State Commun. **11**, 47 (1972).

[20] A. Weber and E. A. McGinnis, J. Mol. Spectrosc. **4**, 195 (1960).

[21] D. W. Posener, Aust. J. Phys. **12**, 184 (1959).

[22] J. J. Olivero and R. L. Longbothum, J. Quant. Spectrosc. Radiat. Transfer **17**, 233 (1977).

[23] J. Menendez and M. Cardona, Phys. Rev. B **29**, 2051 (1984).

[24] J. P. Feser, J. S. Sadhu, B. P. Azeredo, K. H. Hsu, J. Ma, J. Kim, M. Seong, N. X. Fang, X. Li, P. M. Ferreira *et al.* J. Appl. Phys. **112**, 114306 (2012).

[25] J. J. Letcher, K. Kang, D. G. Cahill, and D. D. Dlott, Appl. Phys. Lett., **90**, 252104 (2007).

[26] W. R. Mondal, N. S. Vidhyadhiraja, T. Berlijn, J. Moreno, and M. Jarrell, Phys. Rev. B **96**, 014203 (2017).

[27] P. G. Klemens, Phys. Rev. **148**, 845 (1966).